




# Structure and properties of a quasi-one-dimensional compound BaTiS<sub>3</sub> under pressure

L. C. Fu, W. J. Cheng, Y. Liu, L. C. Shi, Y. Peng, J. Zhang, Z. W. Li, X. D. Li, J. L. Zhu, X. C. Wang & C. Q. Jin


To cite this article: L. C. Fu, W. J. Cheng, Y. Liu, L. C. Shi, Y. Peng, J. Zhang, Z. W. Li, X. D. Li, J. L. Zhu, X. C. Wang & C. Q. Jin (2024) Structure and properties of a quasi-one-dimensional compound BaTiS<sub>3</sub> under pressure, High Pressure Research, 44:2, 95-104, DOI: 10.1080/08957959.2024.2325994

To link to this article: <https://doi.org/10.1080/08957959.2024.2325994>

 View supplementary material 

 Published online: 11 Mar 2024.

 Submit your article to this journal 

 Article views: 131

 View related articles 

 View Crossmark data 



# Structure and properties of a quasi-one-dimensional compound BaTiS<sub>3</sub> under pressure

L. C. Fu<sup>a</sup>, W. J. Cheng<sup>a</sup>, Y. Liu<sup>a</sup>, L. C. Shi<sup>b,c</sup>, Y. Peng<sup>b,c</sup>, J. Zhang<sup>b</sup>, Z. W. Li<sup>b,c</sup>, X. D. Li<sup>d</sup>, J. L. Zhu<sup>a</sup>, X. C. Wang<sup>b,c</sup> and C. Q. Jin<sup>b,c</sup>

<sup>a</sup>Department of Physics, Southern University of Science and Technology, Shenzhen, People's Republic of China; <sup>b</sup>Beijing National Laboratory for Condensed Matter Physics, Institute of Physics, Chinese Academy of Sciences, Beijing, People's Republic of China; <sup>c</sup>School of Physics, University of Chinese Academy of Sciences, Beijing, People's Republic of China; <sup>d</sup>Institute of High Energy Physics, Chinese Academy of Sciences, Beijing, People's Republic of China

## ABSTRACT

We report the studies of structure and properties of a quasi-one-dimensional (quasi-1D) compound BaTiS<sub>3</sub> under pressure. The poly-crystalline samples are synthesized by solid-state reaction method and single-crystalline samples are produced by chemical vapor transport method. The XRD measurement under ambient pressure confirms the hexagonal structure, which consists of face-sharing octahedral TiS<sub>6</sub> chains along *c*-axis and displays a quasi-1D feature. When applying pressure, the synchrotron X-ray diffraction experiments show that the sample undergoes a phase transition from hexagonal phase to orthorhombic phase at around 10 GPa due to the zig-zag deformation of TiS<sub>6</sub> chains, while the quasi-1D structure is reserved. At ambient pressure, BaTiS<sub>3</sub> exhibits an insulating behavior with a band gap about 0.273 eV. When applying pressure, the sample undergoes a crossover from insulator to metal due to the enhancement of inter-chain electron hopping.

## ARTICLE HISTORY

Received 15 November 2023  
Accepted 26 February 2024

## KEYWORDS

Quasi-one-dimensional conductor; electron hopping; high pressure; dimensional crossover

## 1. Introduction

The quasi-one-dimensional (quasi-1D) system exhibits various unique physical phenomena and attracted much research interest due to its low dimensional features. In a quasi-1D conducting system, the Umklapp scattering would have significant impact on the electronic transport and lead to a metal-insulator transition (MIT) [1], and the MIT temperature is dependent on the inter-chain electron hopping [2,3]. As the increase of inter-chain electron hopping, the transition temperature from metallic state to Mott insulating state is gradually suppressed, after which the quasi-1D conducting system would be transformed into three-dimensional metal. During the crossover from 1D to three-

**CONTACT** J. L. Zhu ✉ [zhujl@sustech.edu.cn](mailto:zhujl@sustech.edu.cn) Department of Physics, Southern University of Science and Technology, Shenzhen 518055, People's Republic of China; X. C. Wang ✉ [wangxiancheng@iphy.ac.cn](mailto:wangxiancheng@iphy.ac.cn) Beijing National Laboratory for Condensed Matter Physics, Institute of Physics, Chinese Academy of Sciences, Beijing 100190, People's Republic of China; C. Q. Jin ✉ [jin@iphy.ac.cn](mailto:jin@iphy.ac.cn) Beijing National Laboratory for Condensed Matter Physics, Institute of Physics, Chinese Academy of Sciences, Beijing 100190, People's Republic of China

Supplemental data for this article can be accessed online at <http://dx.doi.org/10.1080/08957959.2024.2325994>.

dimensional (3D) metal, some exotic phenomena may occur, such as charge density wave and superconductivity. This process has been widely investigated in many quasi-1D conducting compounds. For example,  $\text{Li}_{0.9}\text{Mo}_6\text{O}_{17}$  undergoes a dimensional crossover from quasi-1D conductor to a 3D metal at about 24 K. This crossover in dimensionality destabilizes the Luttinger-liquid fixed point and induces an electronic charge (spin) density wave. While further decreasing the temperature, superconductivity can be observed at 1.9 K [3–5].

Another quasi-1D conducting system is  $\text{ABX}_3$  ( $A$  is Ba/Sr,  $B$  is Ti/Zr/Hf and  $X$  is S/Se) [6–13]. They exhibit a hexagonal crystal structure with space group of  $\text{P6}_3/\text{mmc}$ . In this structure, the face-sharing octahedral  $\text{BX}_6$  chains are parallel aligned along the  $c$ -axis and form a triangular lattice in  $ab$ -plane. The large  $A$  atoms separate the  $\text{BX}_6$  chains and resulting in a quasi-1D feature. It has been theoretically predicted that  $\text{BaTiS}_3$  has a typical 1D electron band structure crossing the Fermi surface [14,15]. It should be a metal while it displays insulating behavior under ambient pressure due to the Umklapp scattering effect. Recently, single-crystalline  $\text{BaTiS}_3$  with millimeter-size has been successfully synthesized through chemical vapor transport method with iodine as a transport agent [10,11]. The anisotropic crystal structure and properties indicated that the electron hopping between  $\text{TiS}_6$  chains is much weaker than that of intra-chains. Thus,  $\text{BaTiS}_3$  is a good platform for us to manipulate the inter-chain hopping through applying pressure and explore the 1D related physical phenomena. In this work, we synthesized both poly-crystalline and single-crystalline samples of  $\text{BaTiS}_3$  and measured its crystal structure and transport properties under pressure. A phase transition is observed under high pressure, and the MIT due to the Umklapp scattering effect can be completely suppressed above 20 GPa.

## 2. Materials and methods

### 2.1. Material synthesis

Poly-crystalline samples  $\text{BaTiS}_3$  were prepared by conventional solid-state reaction method. High purity BaS powder (99.2%), Ti powder (99.99%) and S powder (99.99%) were well mixed according to the stoichiometric ratio and pressed into pellets. Then the pellets were placed into alumina crucibles and sealed in evacuated silica tubes. The pellets were heated to  $700^\circ\text{C}$  and held for 20 h before cooling to room temperature. After heating, the poly-crystalline sample  $\text{BaTiS}_3$  can be obtained. Single crystals of  $\text{BaTiS}_3$  were prepared by chemical vapor transport method with iodine as a transport agent. Details of growth method can be seen in [10].

### 2.2. Experimental characterization

#### 2.2.1. Characterization at ambient pressure

The powder X-ray diffraction was conducted on a Rigaku Ultima diffractometer with monochromatic  $\text{Cu-K}_{\alpha 1}$  radiation. The single-crystal X-ray diffraction was conducted on a Bruker D8 VENTURE diffractometer with monochromatic  $\text{Mo-K}_{\alpha 1}$  radiation. The energy-dispersive X-ray spectroscopy (EDX) measurement was carried out on a spectrometer (Model EDAX GENESIS XM2 SYSTEM 60x) equipped with a field-emission scanning electron

microscope (Hitachi S-4800). The electrical resistivity was measured on poly-crystalline sample using the typical four-probe method. The DC magnetization measurement was conducted on a Quantum Design Magnetic Property Measurement System (MPMS).

### 2.2.2. Characterization at high pressure

*In-situ* high pressure angle-dispersive X-ray diffraction measurements were performed at the Beijing Synchrotron Radiation Facility. The X-ray wavelength was 0.6199 Å. A symmetric diamond anvil cell was adopted with the diamond culet being 300 μm in diameter. A prepressed T301 stainless-steel was used as the gasket, and a hole of 150 μm in diameter was drilled as the high pressure chamber. The sample in the chamber was finely grounded poly-crystalline powder and silicon oil was used as the pressure-transfer medium. For the high pressure resistance measurements, a diamond anvil cell made of nonmagnetic BeCu alloy was adopted. The T301 stainless-steel gasket was covered by an insulating layer of *c*-BN powder. NaCl powder was put into the gasket as the pressure-transfer medium (PTM) for transport measurements, which is commonly used although it is non-hydrostatic [16,17]. Single-crystal of BaTiS<sub>3</sub> was used for the high pressure resistance experiments. The pressure was calibrated by the shift of the fluorescence R1 peak of ruby [18] near samples at room temperature for all the experiments.

## 3. Results and discussion

### 3.1. Physical characterization under ambient pressure

Figure 1(a) shows the X-ray diffraction pattern of poly-crystalline BaTiS<sub>3</sub>. All the peaks can be indexed by a hexagonal structure with lattice parameters  $a = b = 6.765(2)$  Å and  $c = 5.793(3)$  Å. The Rietveld refinements for the X-ray diffraction data has been carried out by using GSAS-II software package [19]. By using the space group of P6<sub>3</sub>/mmc as the initial model, the refinements were successfully conducted and smoothly converged to  $R_p = 5.1\%$  and  $R_{wp} = 6.7\%$ , indicating a good fitting. The obtained crystallographic data are summarized in Table S1. The quality of single-crystal BaTiS<sub>3</sub> was determined by EDX and single-crystal XRD. Figure 1(e) shows the EDX spectroscopy measurement results. The synthesized BaTiS<sub>3</sub> single crystals are needle-like in shape with a typical size of 3 mm × 5 μm × 5 μm. The averaged atomic ratio of Ba : Ti : S determined from EDXs is about 1.00(0) : 0.98(3) : 3.07(5), which is close to the stoichiometric ratio within the error range. The single-crystal XRD data were also collected with the sample shown in Figure S1, and the refinement smoothly converged to  $F^2 = 1.170$ ,  $R_1 = 2.6\%$  and  $wR_2 = 6.3\%$  with a model of hexagonal crystal structure (P6<sub>3</sub>/mmc). The refinement results are summarized in Tables 1 and S2. The obtained lattice constants are  $a = b = 6.7670(9)$  Å and  $c = 5.8117(8)$  Å, coincided with the results of poly-crystalline samples.

Figure 1(c,d) shows a sketch of the crystal structure of BaTiS<sub>3</sub> in a top and side views, respectively. We can see that the structure consists of the face-sharing octahedral TiS<sub>6</sub> chains along *c*-axis, which form the triangular lattice in *ab*-plane and are separated by Ba atoms. The nearest Ti–Ti distance in a TiS<sub>6</sub> chain is  $c/2 = 2.906$  Å, much smaller than that of inter-chains given by  $a = 6.767$  Å, thus displaying a quasi-1D structure.

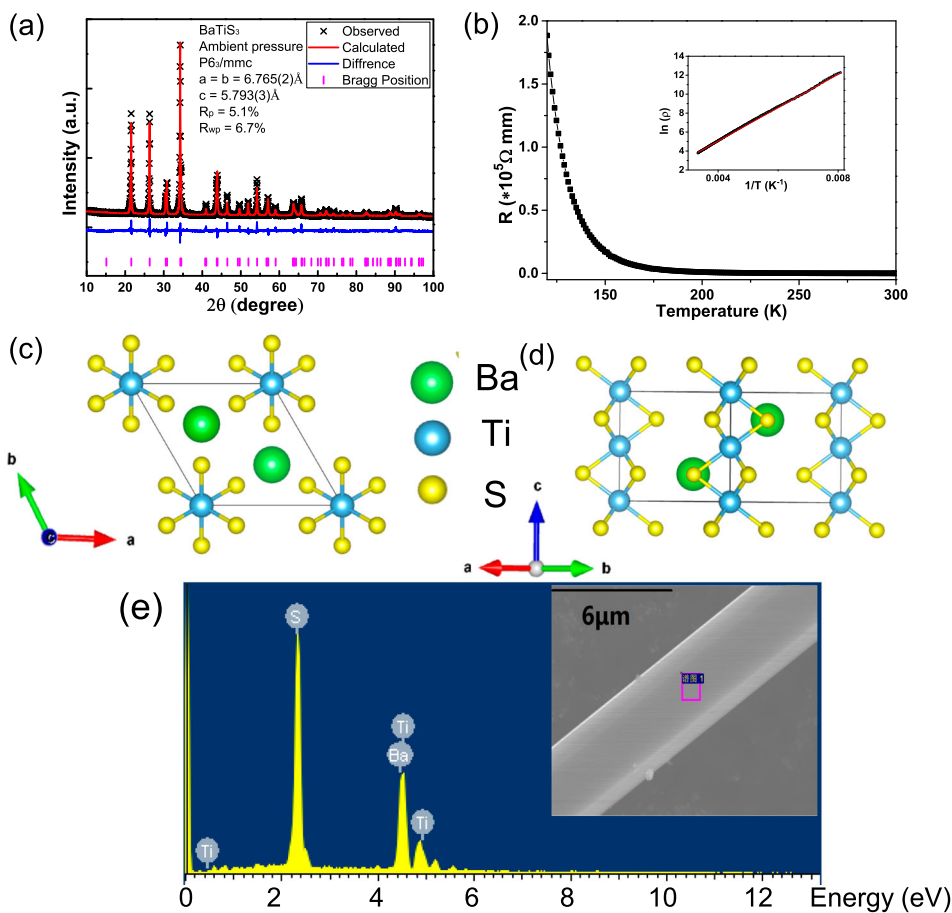


**Figure 1.** (a) The X-ray diffraction patterns and Rietveld refinement of poly-crystalline BaTiS<sub>3</sub>. (b) The temperature dependence of resistivity of poly-crystalline BaTiS<sub>3</sub>. The inset shows the plot of  $\ln(\rho)$  versus the reverse of temperature. (c,d) The sketch of the hexagonal crystal structure in a top and side views, respectively. (e) Energy-dispersive X-ray spectrum for a BaTiS<sub>3</sub> single crystal.

Figure 1(b) shows the temperature dependence of resistivity of poly-crystalline BaTiS<sub>3</sub>. The resistivity increases with decreasing temperature, showing an insulating behavior. The inset shows the plot of  $\ln(\rho)$  versus the reverse of temperature, which displays nearly linear dependence. Hence, the resistivity should follow the Arrhenius law. By fitting the plots with formula  $\rho \propto \exp(\Delta_g/2k_B T)$  ( $\Delta_g$  is the band gap and  $k_B$  is the Boltzmann constant), the band gap is estimated to be 0.273 eV. The insulating behavior is quite common in the quasi-1D conducting system and can be attributed to the Umklapp scattering effect, which usually can induce a metal-insulator transition [20–23].

### 3.2. High pressure synchrotron X-ray diffraction

To exam the structure stability and evolution of BaTiS<sub>3</sub> under high pressure, we conduct the *in-situ* high pressure angle-dispersive X-ray diffraction measurement on BaTiS<sub>3</sub> powders at room temperature. Figure 2(a) shows the XRD patterns measured under

**Table 1.** Crystallographic data for hexagonal and orthorhombic phase of BaTiS<sub>3</sub>.

BaTiS <sub>3</sub> (single-crystal, ambient pressure)						BaTiS <sub>3</sub> (poly-crystal, 29.9 GPa)					
Space group: P6 <sub>3</sub> /mmc						Space group: Cmc21					
$a = b = 6.7670(9) \text{ \AA}, c = 5.8117(8) \text{ \AA}, \alpha = \beta = 90^\circ, \gamma = 120^\circ$						$a = 6.254(8) \text{ \AA}, b = 10.565(9) \text{ \AA}, c = 5.349(5) \text{ \AA}, \alpha = \beta = \gamma = 90^\circ$					
$R_1 = 2.6\%$ and $wR_2 = 6.3\%$						$R_p = 6.8\%$ and $R_{wp} = 9.7\%$					
Atom	fraction	<i>x</i>	<i>y</i>	<i>z</i>	<i>U</i>	Atom	fraction	<i>x</i>	<i>y</i>	<i>z</i>	<i>U</i>
S	1	0.66803	-0.16602	0.25000	0.0403	S2	1	0.27801	0.41995	0.02862	0.0135
Ba	1	0.66667	0.33333	0.25000	0.0295	Ti	1	0.00000	0.02598	0.25222	0.0228
Ti	1	1.00000	0.00000	0.50000	0.0731	S1	1	0.00000	0.16289	0.01313	0.0374
						Ba	1	0.00000	0.33529	0.50715	0.0260

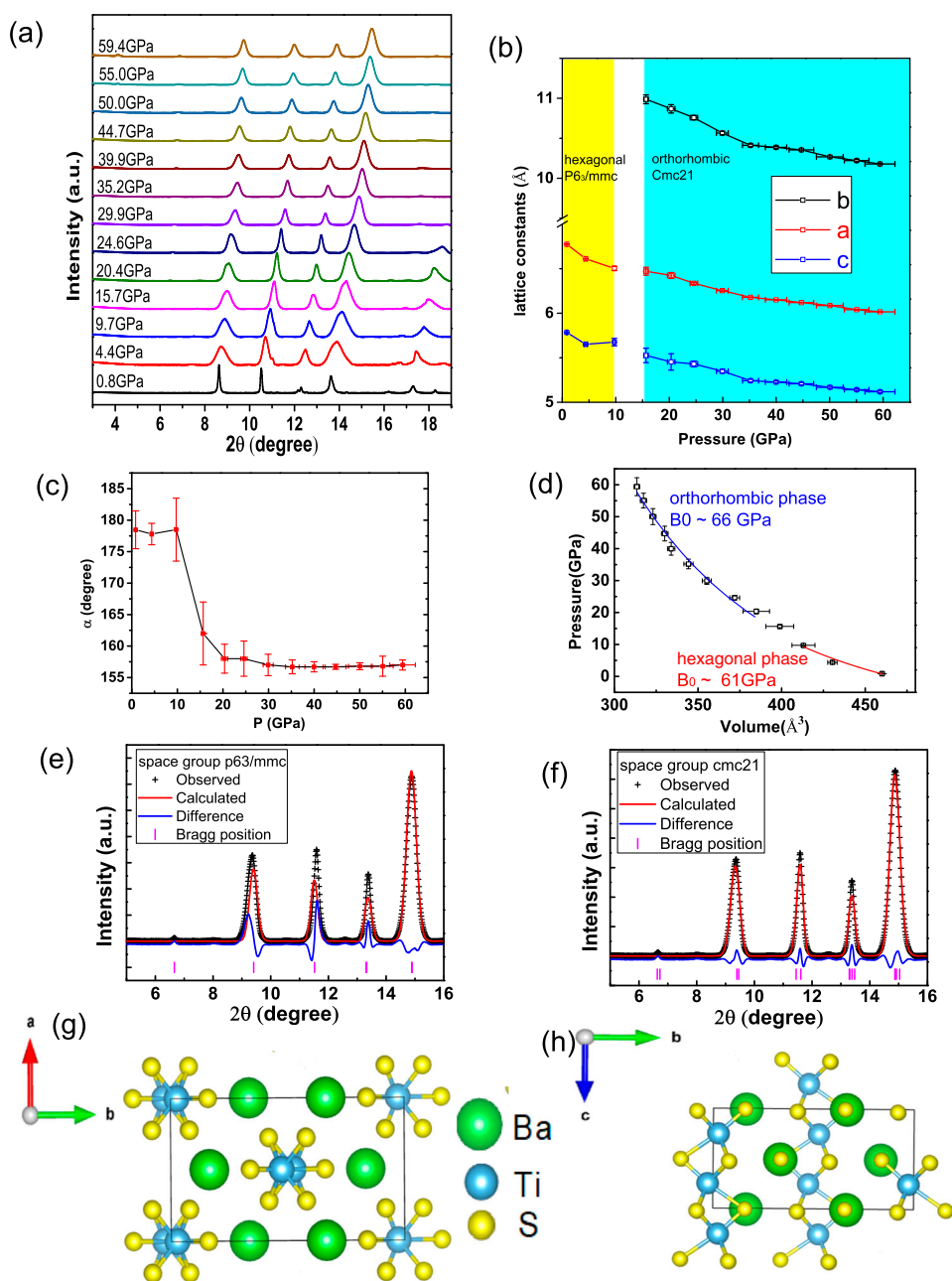


**Figure 2.** (a) The XRD patterns measured under different pressures. (b) The pressure dependence of crystal lattice constants. (c) The  $\alpha$  (the angle of Ti-Ti-Ti in a TiS<sub>6</sub> chain) versus pressure plots. (d) The pressure versus cell volume plots and the fitting using Birch–Murnaghan equation. (e)(f) The refinement results of the XRD patterns measured under 29.9 GPa using the hexagonal and orthorhombic crystal structure, respectively. (g)(h) The sketch of the orthorhombic crystal structure of BaTiS<sub>3</sub> in a top and side views, respectively.

different pressures. Within the highest experimental pressure of 59.4 GPa, all the peaks shift gradually to the high angle region while increasing pressure and no new peaks were found, indicating the shrink of lattice under pressure. We try to use the space group of  $P6_3/mmc$  as the initial model to carry out the refinements. This model works well in the low-pressure region. However, the positions of the calculated peaks gradually show mismatch with the positions of the observed peaks measured at high pressures, as seen in [Figure 2\(e\)](#). We note that  $BaVS_3$ , which shares the same crystal structure with  $BaTiS_3$  at room temperature, undergoes a transition from hexagonal to orthorhombic structure (space group of  $Cmc21$ ) with decreasing temperature [24,25]. Similar phase transition has also been observed in  $BaVSe_3$  [26]. Usually, the low-temperature phase can be realized by applying high pressure at room temperature as seen in  $NaBH_4$  [27]. Thus, we use the low-temperature phase of  $BaVSe_3$  as the initial structure model to carry out the refinements for the high pressure X-ray diffraction data, and the refinements converge to reasonable  $R$ -values of  $R_p = 6.8\%$  and  $R_{wp} = 9.7\%$ . The obtained crystallographic data for  $BaTiS_3$  with orthorhombic phase are summarized in [Table 1](#). In [Figure 2\(e,f\)](#), as an example, we show the refinement results of the data measured under 29.9 GPa using the hexagonal and orthorhombic structure, respectively. Apparently, the latter shows a better fitting.

[Figure 2\(g,h\)](#) shows the sketch of the orthorhombic crystal structure of  $BaTiS_3$  in a top and side views, respectively. Compared with the hexagonal structure, they are nearly the same except for the distortion of the  $TiS_6$  chains. That is, in the hexagonal structure, the Ti atoms located exactly along the  $c$ -axis in a  $TiS_6$  chain; while in the orthorhombic crystal structure, the Ti atoms exhibit a zig-zag like chain, while the quasi-1D structure is reserved. Thus, the hexagonal structure can be viewed as a specialized orthorhombic structure with  $\alpha = 180^\circ$  (the angle of Ti–Ti–Ti in a  $TiS_6$  chain). To describe the distortion under different pressures, we did the refinements with orthorhombic crystal structure for all the data measured under pressures. [Figure 2\(c\)](#) shows the pressure dependence of  $\alpha$ . The value of  $\alpha$  is quite close to  $180^\circ$  with pressure lower than 9.7 GPa, while it decreases quickly when the pressure exceeds 9.7 GPa and finally converged to about  $157^\circ$ , indicating that a phase transition happens at about 10 GPa. The pressure dependences of lattice constants and volume are also shown in [Figure 2\(b,d\)](#). The lattice constants decrease with increasing pressure and are compressed by about 11.3% and 11.7% for  $a$  and  $c$  within 59.4 GPa, respectively, indicating an isotropic compression. Especially, the decrease of  $a$ , which is equal to the distance between nearest  $TiS_6$  chains, suggests an enhancement of the inter-chain electron hopping. In [Figure 2\(d\)](#), the pressure versus volume is also plotted and fitted by Birch–Murnaghan equation  $P(\text{GPa}) = 3/2 \times B_0[(V_0/V)^{2/3} - (V_0/V)^{5/3}] \times \{1 - (3 - 3/4 \times B'_0) \times [(V_0/V)^{2/3} - 1]\}$  with  $B'_0$  fixed as 4, giving a bulk modulus of  $B_{0h} \sim 61$  GPa for the low-pressure hexagonal phase and  $B_{0o} \sim 66$  GPa for the high pressure orthorhombic phase.

### 3.3. High pressure transport properties

[Figure 3\(a–c\)](#) shows the temperature dependence of resistance measured along the  $c$ -axis of single-crystalline  $BaTiS_3$  sample under different pressures with temperature down to 2 K. At 3.0 GPa, the resistance decreases with increasing temperature, demonstrating an insulating behavior in the measured temperature range. While for the data measured



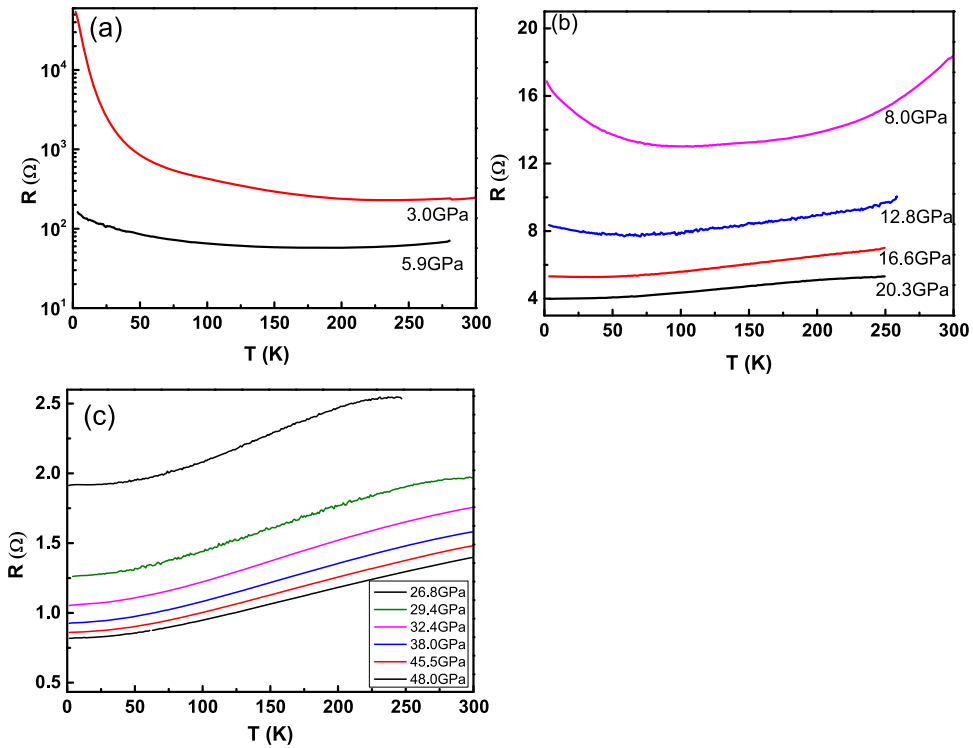


**Figure 3.** (a–c) Temperature dependence of the resistance measured under different pressures.

under 5.9 GPa, it shows a metallic behavior at high temperature and a MIT transition occurs at about 170 K. Further increasing pressure, this MIT temperature is gradually suppressed as can be clearly seen in Figure S2, and it becomes a complete metal above 20 GPa. Within the pressure of 48 GPa, no superconductivity is observed above 2 K. Theoretical studies have revealed that  $\text{BaTiS}_3$  is a typical 1D metal along the  $c$ -axis [14,15], while an insulating behavior measured along the  $c$ -axis is observed at low pressures. It implies that the Umklapp scattering effect has played a key role for the MIT. When the applied pressure increases, the distance between the conducting chains of  $\text{TiS}_6$  is gradually decreased, which should enhance the electron hopping between the conducting chains and weaken the Umklapp scattering effect. Thus, the suppression of MIT by pressure demonstrates an intrinsic property for  $\text{BaTiS}_3$  with 1D conducting chains.

#### 4. Conclusions

In conclusion, we have prepared both the poly-crystalline and single-crystalline samples of  $\text{BaTiS}_3$ . At ambient pressure, it has a hexagonal crystal structure, which consists of well separated face-sharing octahedral  $\text{TiS}_6$  chains and exhibits a quasi-1D structure characteristic. The resistivity measurement at ambient pressure confirms the insulating behavior with a band gap about 0.273 eV. When applying pressure,  $\text{BaTiS}_3$  undergoes a phase transition from hexagonal phase to orthorhombic phase at around 10 GPa due to the zig-zag deformation of  $\text{TiS}_6$  chains. The quasi-1D structure is reserved and the distance between  $\text{TiS}_6$

chains decreases with increasing pressure, indicating the enhancement of the inter-chain electron hopping. With increasing pressure, the resistance shows metal to insulator transition and the MIT temperature gradually decreases, and a complete metallic behavior can be realized above 20.3 GPa, which demonstrates an intrinsic property for BaTiS<sub>3</sub> with 1D conducting chains.

## Acknowledgments

J. Z. also acknowledged the Major Science and Technology Infrastructure Project of Material Genome Big-science Facilities Platform supported by Municipal Development and Reform Commission of Shenzhen. Some experiments are supported by the Synergic Extreme Condition User Facility.

## Data availability statement

The data that support the findings of this study are available from the corresponding author upon reasonable request.

## Disclosure statement

No potential conflict of interest was reported by the authors.

## Funding

This work was supported by the National Key R&D Program of China and the Natural Science Foundation of China [grant numbers 12004161, 2023YFA1406001 and 12274193], the Stable Support Plan Program of Shenzhen Natural Science Fund [grant number 20200925152415003], the Project funded by the Basic and Applied Basic Research Foundation of Guangdong Province [grant number 2022A1515010044].

## References

- [1] Giamarchi T. Mott transition in one dimension. *Phys B: Condens Matter*. 1997;230:975–980. doi: [10.1016/S0921-4526\(96\)00768-5](https://doi.org/10.1016/S0921-4526(96)00768-5)
- [2] Giamarchi T. Theoretical framework for quasi-one dimensional systems. *Chem Rev*. 2004;104(11):5037–5056. doi: [10.1021/cr030647c](https://doi.org/10.1021/cr030647c)
- [3] Biermann S, Georges A, Lichtenstein A, et al. Deconfinement transition and luttinger to fermi liquid crossover in quasi-one-dimensional systems. *Phys Rev Lett*. 2001;87(27):276405. doi: [10.1103/PhysRevLett.87.276405](https://doi.org/10.1103/PhysRevLett.87.276405)
- [4] Filippini CE, Beille J, Boujida M, et al. Pressure effect on the transport properties of superconducting Li<sub>0.9</sub>Mo<sub>6</sub>O<sub>17</sub> bronze. *Phys C Supercond Appl*. 1989;162:427–428. doi: [10.1016/0921-4534\(89\)91088-5](https://doi.org/10.1016/0921-4534(89)91088-5)
- [5] Mercure JF, Bangura A, Xu X, et al. Upper critical magnetic field far above the paramagnetic pair-breaking limit of superconducting one-dimensional Li<sub>0.9</sub>Mo<sub>6</sub>O<sub>17</sub> single crystals. *Phys Rev Lett*. 2012;108(18):187003. doi: [10.1103/PhysRevLett.108.187003](https://doi.org/10.1103/PhysRevLett.108.187003)
- [6] Clearfield A. The synthesis and crystal structures of some alkaline earth titanium and zirconium sulfides. *Acta Crystallogr*. 1963;16(2):135–142. doi: [10.1107/S0365110X6300030X](https://doi.org/10.1107/S0365110X6300030X)
- [7] Huster J. Die kristallstruktur von BaTiS<sub>3</sub>/crystal structure of BaTiS<sub>3</sub>. *Z Fur Naturforsch B*. 1980;35(6):775–775. doi: [10.1515/znb-1980-0630](https://doi.org/10.1515/znb-1980-0630)

- [8] Niu S, Zhao H, Zhou Y, et al. Mid-wave and long-wave infrared linear dichroism in a hexagonal perovskite chalcogenide. *Chem Mater.* 2018;30(15):4897–4901. doi: [10.1021/acs.chemmater.8b02279](https://doi.org/10.1021/acs.chemmater.8b02279)
- [9] Niu S, Huyan H, Liu Y, et al. Band-gap control via structural and chemical tuning of transition metal perovskite chalcogenides. preprint, 2018. arXiv:180409362.
- [10] Zhao B, Hoque MSB, Jung GY, et al. Orientation-controlled anisotropy in single crystals of quasi-1d BaTiS<sub>3</sub>. *Chem Mater.* 2022;34(12):5680–5689. doi: [10.1021/acs.chemmater.2c01046](https://doi.org/10.1021/acs.chemmater.2c01046)
- [11] Niu S, Joe G, Zhao H, et al. Giant optical anisotropy in a quasi-one-dimensional crystal. *Nat Photon.* 2018;12(7):392–396. doi: [10.1038/s41566-018-0189-1](https://doi.org/10.1038/s41566-018-0189-1)
- [12] Meng W, Saparov B, Hong F, et al. Alloying and defect control within chalcogenide perovskites for optimized photovoltaic application. *Chem Mater.* 2016;28(3):821–829. doi: [10.1021/acs.chemmater.5b04213](https://doi.org/10.1021/acs.chemmater.5b04213)
- [13] Perera S, Hui H, Zhao C, et al. Chalcogenide perovskites—an emerging class of ionic semiconductors. *Nano Energy.* 2016;22:129–135. doi: [10.1016/j.nanoen.2016.02.020](https://doi.org/10.1016/j.nanoen.2016.02.020)
- [14] Paudel TR, Tsymbal EY. Evaluating the thermoelectric properties of BaTiS<sub>3</sub> by density functional theory. *ACS Omega.* 2020;5(21):12385–12390. doi: [10.1021/acsomega.0c01139](https://doi.org/10.1021/acsomega.0c01139)
- [15] Mathew T, Joseph S, Mathew V, et al. Density functional study of structural, electronic and optical properties of quasi-one-dimensional compounds BaTiX<sub>3</sub> (X = S, Se). *Superlattices Microstruct.* 2021;153:106859. doi: [10.1016/j.spmi.2021.106859](https://doi.org/10.1016/j.spmi.2021.106859)
- [16] Errandonea D, Meng Y, Somayazulu M, et al. Pressure-induced  $\alpha \rightarrow \omega$  transition in titanium metal: a systematic study of the effects of uniaxial stress. *Phys B: Condens Matter.* 2005;355(1–4):116–125. doi: [10.1016/j.physb.2004.10.030](https://doi.org/10.1016/j.physb.2004.10.030)
- [17] Errandonea D, Segura A, Martínez-García D, et al. Hall-effect and resistivity measurements in CdTe and ZnTe at high pressure: electronic structure of impurities in the zinc-blende phase and the semimetallic or metallic character of the high pressure phases. *Phys Rev B.* 2009;79(12):125203. doi: [10.1103/PhysRevB.79.125203](https://doi.org/10.1103/PhysRevB.79.125203)
- [18] Shen G, Wang Y, Dewaele A, et al. Toward an international practical pressure scale: a proposal for an IPPS ruby gauge (IPPS-Ruby2020). *High Press Res.* 2020;40(3):299–314. doi: [10.1080/08957959.2020.1791107](https://doi.org/10.1080/08957959.2020.1791107)
- [19] Toby BH, Von Dreele RB. GSAS-II: the genesis of a modern open-source all purpose crystallography software package. *J Appl Crystallogr.* 2013;46(2):544–549. doi: [10.1107/S0021889813003531](https://doi.org/10.1107/S0021889813003531)
- [20] Giamarchi T. Umklapp process and resistivity in one-dimensional fermion systems. *Phys Rev B.* 1991;44(7):2905. doi: [10.1103/PhysRevB.44.2905](https://doi.org/10.1103/PhysRevB.44.2905)
- [21] Vescoli V, Degiorgi L, Henderson W, et al. Dimensionality-driven insulator-to-metal transition in the bechgaard salts. *Science.* 1998;281(5380):1181–1184. doi: [10.1126/science.281.5380.1181](https://doi.org/10.1126/science.281.5380.1181)
- [22] Zhang J, Jia Y, Wang X, et al. A new quasi-one-dimensional compound Ba<sub>3</sub>TiTe<sub>5</sub> and superconductivity induced by pressure. *NPG Asia Mater.* 2019;11(1):60. doi: [10.1038/s41427-019-0158-2](https://doi.org/10.1038/s41427-019-0158-2)
- [23] Pashkin A, Dressel M, Kuntscher CA. Pressure-induced deconfinement of the charge transport in the quasi-one-dimensional mott insulator (TMTTF)<sub>2</sub>AsF<sub>6</sub>. *Phys Rev B.* 2006;74(16):165118. doi: [10.1103/PhysRevB.74.165118](https://doi.org/10.1103/PhysRevB.74.165118)
- [24] Gardner R, Vlasse M, Wold A. Preparation, properties and crystal structure of barium vanadium sulfide, BaVS<sub>3</sub>. *Acta Crystallogr B: Struct Sci Cryst.* 1969;25(4):781–787. doi: [10.1107/S0567740869002962](https://doi.org/10.1107/S0567740869002962)
- [25] Fagot S, Foury-Leylekan P, Ravy S, et al. Structural aspects of the metal-insulator transition in BaVS<sub>3</sub>. *Solid State Sci.* 2005;7(6):718–725. doi: [10.1016/j.solidstatesciences.2004.11.017](https://doi.org/10.1016/j.solidstatesciences.2004.11.017)
- [26] Kelber J, Reis Jr A, Aldred A, et al. Structural and magnetic properties of ‘one-dimensional’ barium vanadium triselenide. *J Solid State Chem.* 1979;30(3):357–364. doi: [10.1016/0022-4596\(79\)90248-2](https://doi.org/10.1016/0022-4596(79)90248-2)
- [27] Sundqvist B, Andersson O. Low-temperature phase transformation in NaBH<sub>4</sub> under pressure. *Phys Rev B.* 2006;73(9):092102. doi: [10.1103/PhysRevB.73.092102](https://doi.org/10.1103/PhysRevB.73.092102)